Full Bridge LLC Resonant Converter Design for Photovoltaic Applications

Tufan Volkan Küçük
Department of Electric, Osmaneli Vocational High School
Bilecik Seyh Edebali University
Bilecik, Turkey
tufan.kucuk@bilecik.edu.tr

Selim Öncü
Department of Electrical and Electronics Eng.
Karabuk University
Karabuk, Turkey
soncu@karabuk.edu.tr

***Abstract*—In this study, full bridge LLC resonant converter is simulated for photovoltaic (PV) system. The maximum power point tracking (MPPT) algorithm perturb and observe (P&O) is used to tracking the maximum power point (MPP) in the PV system at different irradiance values. P&O algorithm is modified for phase shift modulation and made suitable for resonant converter. The proposed system is simulated under three different irradiance values. It can be seen from the simulation results that MPPT and soft switching conditions have been successfully achieved in all three irradiance values.**

Keywords—PV system, LLC resonant converter, Maximum power point tracking, Phase shift modulation.

I. INTRODUCTION

Fossil fuels are energy sources with limited reserves and are expected to be depleted in the near future. In addition, in the process of obtaining electrical energy using fossil fuels, gases that are harmful to the environment and human health are released. Considering that global warming is an undeniable fact, it is seen that the importance of renewable energy sources is increasing day by day. Among renewable energy sources, PV systems stand out as the primary energy source for the supply of electrical energy, especially in regions without grid connection.

PVs are systems that can produce electrical energy depending on the amount of radiation in the sun. DC-DC converters are critical in processing the direct current obtained from PV panels and transferring it to another converter or load in a controlled manner [1]. One of the main tasks of these converters is to arrange the PV system to operate at the MPP at different solar irradiance levels [1,2]. In addition, it is expected that the converters will increase the reliability of the system and operate at high efficiency by reducing the leakage to the ground caused by the PV panel parasitic capacitance effect [1,2]. Among the DC-DC converter topologies used in PV systems, traditional pulse width modulated converters (Buck, Boost, Buck-boost, Cuk) are frequently preferred with their simple structures and low costs [1-3]. However, in case of low frequency switching in these converter topologies, the dimensions and costs of the passive circuit elements increase and the power density decreases [2,3]. In case of using high frequency, switching losses increase due to hard switching. In addition, electromagnetic interference (EMI) noises occur and voltage stresses happen on the power switches, thus reducing the efficiency [3-5].

Because of the above mentioned results, many researchers focus on resonant power converters [6]. Resonant converters reduce switching losses by changing the operating of power switches at zero voltage (ZVS) and/or zero current (ZCS). The realization of soft switching allows the designed power converter to operate at high frequencies. Thus, the dimensions and costs of passive circuit elements are reduced and the power density increases. EMI effects are also reduced by soft switching [4-6].

Many different resonant converters are studied in the literature. Two-element series resonant converters (SRC) are preferred because of their high efficiency. However, it causes output voltage regulation problems at low load currents [6]. Two-element parallel resonant converters (PRC) have higher voltage regulation capability than SRCs at low load currents. The resonant tank current in PRCs is independent of the load and is higher than in SRCs. This situation negatively affects the efficiency due to conduction losses, especially at low load currents [7]. Three-element serial-parallel resonant converters (SPRC) have the advantages of SRC and PRC converters. Circulating currents are lower than PRCs, and output voltage regulation capabilities at low load currents are higher than SRCs [6,7]. Two basic topology are frequently used in SPRCs. These are the LCC and LLC converter topologies. LCC converters are preferred especially in applications where high output voltage is required due to their high DC voltage gain characteristics. Among the mentioned resonant converters, LLC resonant converters get more attention in PV systems due to their high efficiency, low circulation energy and ability to provide ZVS condition in a wide operating range [6-8]. LLC resonant converters designed for PV systems have been analyzed in terms of control methods. In [9], the output voltage of the resonant converter is regulated using the pulse frequency modulation method. The incremental conductance (INC) algorithm used as the MPPT method is designed to work with frequency modulation. Variable frequency control, despite the ease of application, causes the magnetic design to be complex and the EMI level to increase. In [10], a full-bridge LLC converter control was performed using the phase shift control method. The perturb and observe (P&O) MPPT algorithm is arranged according to the phase shift control method. Phase shift control has made it possible to operate at a constant switching frequency. Thus, the magnetic design challenges and EMI problems are reduced. A similar study is presented in [6]. In both studies, the soft switching conditions under different irradiance values are not clearly expressed. In [11], two PV panels were operated at MPP using a dual half-bridge LLC resonant converter. The overall system performance was improved by using phase shift and frequency modulation methods. in [12], in addition to phase shift and frequency modulation methods, pulse skipping method was added to increase system efficiency at low load currents, but the control structure became more complex.

In this study, the analysis of a full bridge LLC resonant converter powered by a PV panel was carried out. The resonant converter is controlled at a constant switching frequency and by the phase shift modulation method. P&O

algorithm has been used so that the PV panel can operate at the MPP under different irradiance values. The P&O algorithm was revised to determine the phase shift angle and adapted to the resonant converter. MPPT and soft switching capability of the designed system under different irradiance values were investigated by using PSIM simulation program.

II. Full Bridge LLC Resonant Converter

The full bridge LLC resonant converter circuit diagram is presented in Fig. 1. The resonant converter consists of three main parts: full bridge inverter, LLC resonant tank and rectifier. The full-bridge inverter consists of four power switches and is named S1-S4 in Fig. 1.

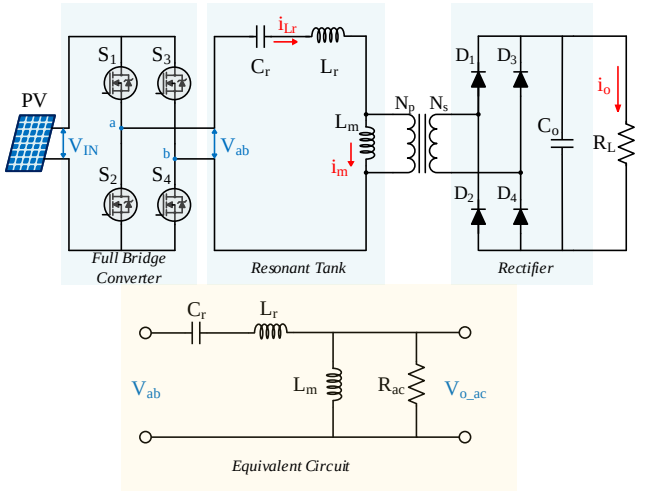

Fig. 1. Full bridge LLC resonant converter circuit

The DC voltage obtained from the PV panel is converted into a square wave with a full-bridge inverter and transferred to the LLC resonant tank. The resonant tank circuit consists of the resonant inductance (L_r), the magnetization inductance (L_m) and the resonant capacitor C_r elements. D1-D4 represent power diodes. The alternating voltage at the output of the resonant tank circuit is rectified by the full bridge rectifier and transferred to the load. The capacitor used as the output load filter is shown by the symbols C_o and the output load current is shown by the symbols i_o. In Fig. 1, i_{Lr} current refers to the current passing through L_r, and i_m represents to the magnetization current of the transformer. N_p and N_s symbolize the primary and secondary windings of the transformer, respectively. If the conversion ratio of the transformer is n, it is calculated with N_p/N_s [13-15]. The LLC resonant converter has two different resonance frequencies depending on whether the inductance L_m is included in the series resonant circuit or not. Both resonance frequencies are calculated by (1) [13].

$$f_{r1} = \frac{1}{2\pi\sqrt{L_r \cdot C_r}}$$
$$f_{r2} = \frac{1}{2\pi\sqrt{(L_r + L_m) \cdot C_r}} \quad (1)$$

R_{ac}, which is the load resistance R_L transferred to the resonant equivalent circuit depending on the conversion ratio of the transformer (n), is calculated by (2).

$$R_{ac} = \frac{8}{\pi^2} \cdot n^2 \cdot R_L \quad (2)$$

The quality factor (Q) of the LLC resonant circuit is calculated by (3).

$$Q = \frac{\sqrt{L_r / C_r}}{R_{ac}} \quad (3)$$

The normalized frequency (F_x) is calculated by (4).

$$F_x = \frac{f_{sw}}{f_{r1}} \quad (4)$$

The inductance ratio m is calculated by (5)

$$m = \frac{L_r + L_m}{L_r} \quad (5)$$

In the equivalent circuit given in Fig. 1, the ratio of the output voltage (V_{o_ac}) to the input voltage (V_{ab}) gives the gain of the resonance circuit. In (6), the calculation of the gain function K is given depending on the quality factor, inductance ratio and normalized frequency value.

$$K(Q, m, F_x) = \left| \frac{F_x^2 \cdot (m-1)}{\sqrt{\left(m \cdot F_x^2 - 1\right)^2 + F_x^2 \cdot \left(F_x^2 - 1\right)^2 \cdot (m-1)^2 \cdot Q^2}} \right| \quad (6)$$

The operating regions of a basic LLC resonance circuit with constant m value and gain curves according to different Q values are presented in Fig. 2.

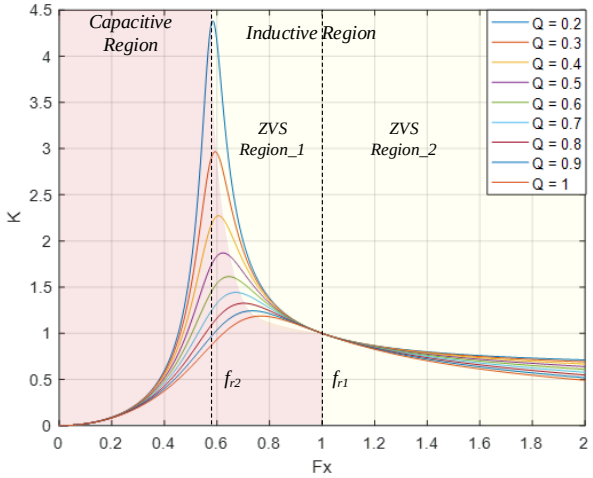

Fig. 2. Gain curve of a general LLC resonant converter circuit.

When L_r and C_r values are taken as constant, the quality factor changes with the load resistance. While the low load resistance increases the Q value, the high load resistance decreases the Q value. Fig. 2 shows the operating region of a typical LLC resonant circuit [14,15]. The red shaded area shows the region where the resonant circuit has capacitive character. In this region, the resonant circuit has capacitive impedance and the resonant current is ahead of the resonant

voltage. In the capacitive region, turning on of power switches occurs under hard switching conditions. Therefore, work in the capacitive zone is avoided. In the yellow region (ZVS Region_1) between the two resonance frequencies, the resonant circuit shows an inductive feature. In the operation realized in this region, the power switches meet the ZVS condition, while the power diodes operate under ZCS conditions. At switching frequencies above the resonant frequency f_{r1} (ZVS Zone_2), the resonant circuit maintains its inductive feature. In this region, the power switches satisfy the ZVS condition, while the power diodes lose their ZCS feature [16,17]. If the switching frequency (f_s) is selected to equal f_{r1}, the resonant impedance value becomes zero and the circuit shows ohmic characteristic. Thus, maximum power transfer to the output is realized.

III. Phase Shift Modulation

Control of full bridge LLC resonant converter with phase shift modulation method is presented in Fig. 3. In the full-bridge inverter, the gate signals applied to the switches S1 and S2 are inverted relative to each other. Similarly, switches S3 and S4 are inverted relative to each other [13,18]. In addition, dead time is added to prevent the upper and lower switches from conducting at the same time. In the phase shift modulation method, the duty ratio of all power switches is fixed and 0.5. The phase shift angle is defined by β. S1 and S2 switches are fixed, while S3 and S4 switches are phase shifted. The voltage V_{ab} reaches its maximum value when the β is 180°. As the angle value decreases, the effective value of the V_{ab} voltage decreases [15,19]. Fig. 3 presents the gate signals of the S1 and S3 switches and the shapes of the V_{ab} output voltage signal in the case of (a) 180° (b) 135° (c) 90° and (d) 45° phase shift angles (β).

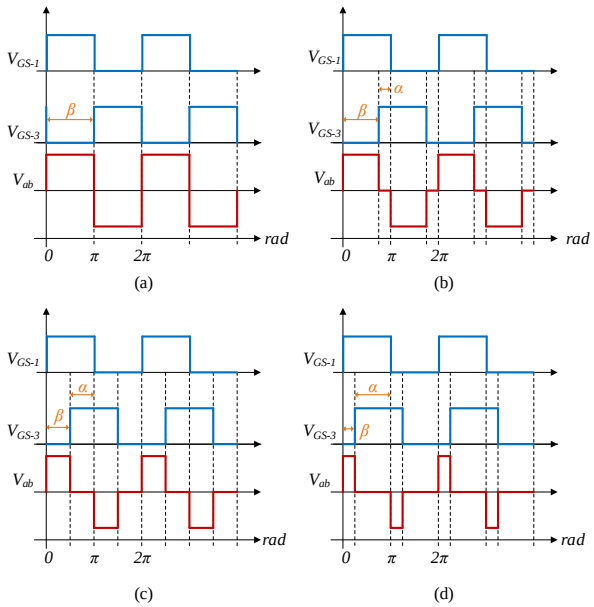

Fig. 3. Control of full-bridge inverter with phase shift modulation.

The fundamental harmonic approximation (FHA) method is frequently preferred in the analysis of the LLC resonant converter, especially in studies close to the resonant frequency. This analysis technique is based on the fundamental harmonic in the Fourier series expansion of the square wave voltage V_{ab} applied to the resonant tank. While applying the FHA method, high order harmonics of the primary and secondary voltages and currents of the transformer and the leakage inductances of passive circuit elements such as capacitors and inductors are neglected. The Fourier expansion of the resonant tank input voltage is expressed by (7).

$$V_{ab}(t) = \frac{4 \cdot V_{IN}}{\pi} \sum_{n=1,3,5,\ldots}^{\infty} \frac{1}{n} \cdot \sin(2\pi n f_s t) \tag{7}$$

The fundamental component of the V_{ab} can be calculated by (8)

$$V_{ab\_1}(t) = \frac{4 \cdot V_{IN}}{\pi} \cdot \sin(2\pi f_s t) \tag{8}$$

Depending on the β and α angles, the fundamental component of the voltage V_{ab} is given by (9).

$$\begin{aligned} V_{ab\_1}(t) &= \frac{4 \cdot V_{IN}}{\pi} \cdot \sin\left(\frac{\beta}{2}\right) \cdot \sin(2\pi f_s t) \\ V_{ab\_1}(t) &= \frac{4 \cdot V_{IN}}{\pi} \cdot \cos\left(\frac{\alpha}{2}\right) \cdot \sin(2\pi f_s t) \end{aligned} \tag{9}$$

IV. MPPT Algorithm

Among the MPPT algorithms used in PV systems, P&O and INC algorithms are frequently preferred due to their simple structure and not needing the data of environmental conditions.

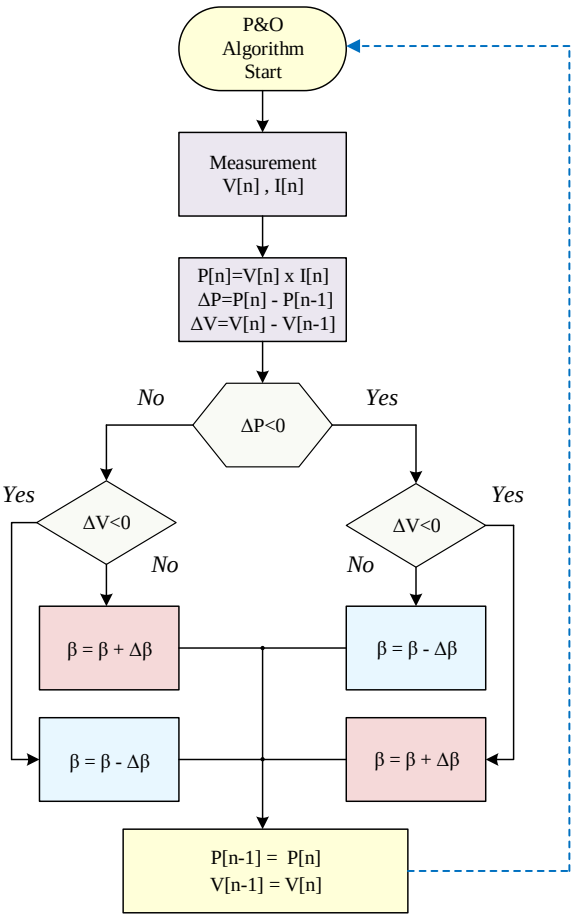

Fig. 4. Proposed P&O Algorithm flowchart.

P&O algorithm is used as MPPT algorithm in the designed system. In the P&O algorithm, instantaneous power is calculated using the voltage and current information obtained from the PV panel. The power change is determined by comparing the current power with the power obtained from the previous measurement [21]. At the second stage, the voltage change is detected. The phase shift angle is increased or decreased according to whether the voltage change is positive or negative [6]. Figure 4 presents the flow diagram of the P&O Algorithm. In the traditional P&O algorithm, the duty ratio is controlled to ensure that the system works in MPP, while the β is controlled in the proposed algorithm.

V. Simulation Results

The simulation of the designed system was carried out using the PSIM program. Table 1 presents the electrical characteristics of the full bridge LLC resonant converter and the PV panel. In the simulated system, the maximum power of the PV panel under 1000W/m^2 irradiance is 325.7 W.

TABLE I. ELECTRICAL PARAMETERS OF THE DESIGNED SYSTEM

PV Panel Parameters		
Open-circuit voltage	V_{oc}	45,11 V
Short-circuit current	I_{sc}	9,31 A
MPP voltage	V_{mp}	37,28 V
MPP current	I_{mp}	8,72 A
*All values are valid for 1000 w/m^2 irradiance and 25 °C temperature.		
Full Bridge LLC Converter Parameters		
Resonance inductance	L_r	5,45 µH
Magnetizing inductance	L_m	27,25 µH
Resonance capacior	C_r	0,47 µF
Fiter capacitor	C_o	100 µF
Load	R_L	400 Ω
Resonance frequency	f_{r1}	100 kHz
Switching frequency	f_{sw}	100 kHz
Transformer ratio	n (N_p/N_s)	0,1

The full circuit model of the PSIM simulation program is presented in Fig. 5. The switching frequency of the full-bridge LLC converter is chosen equal to the resonant frequency

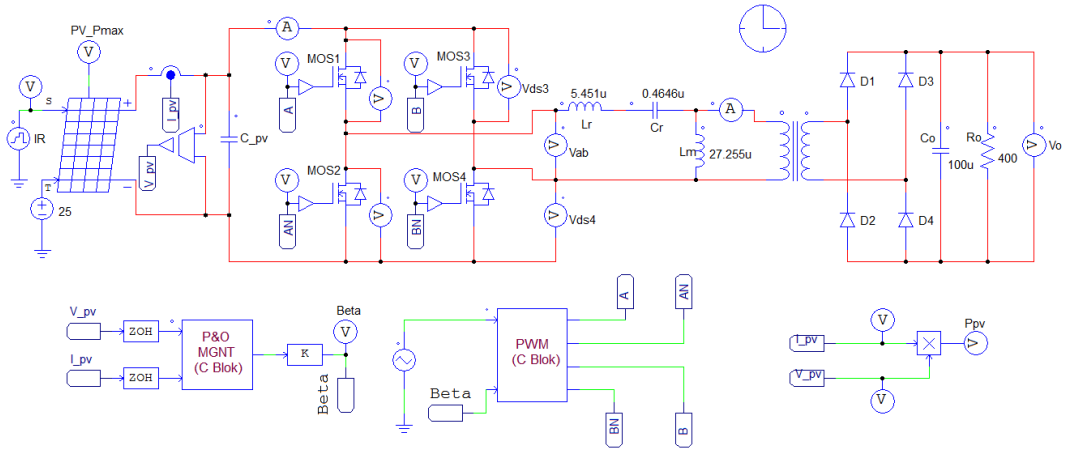

Fig. 5. PSIM model of the simulated PV system.

The Figure 6 presents the theoretical maximum power (PV_Pmax) and instantaneous maximum power (Ppv) of the PV panel under the solar irradiance value (IR) of 300-1000-750 W/m^2.

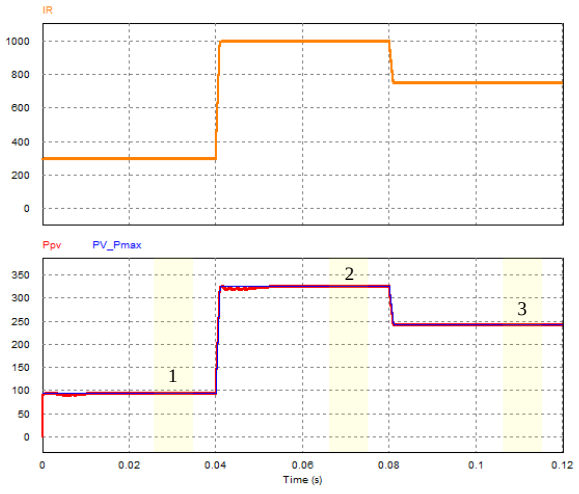

(a)

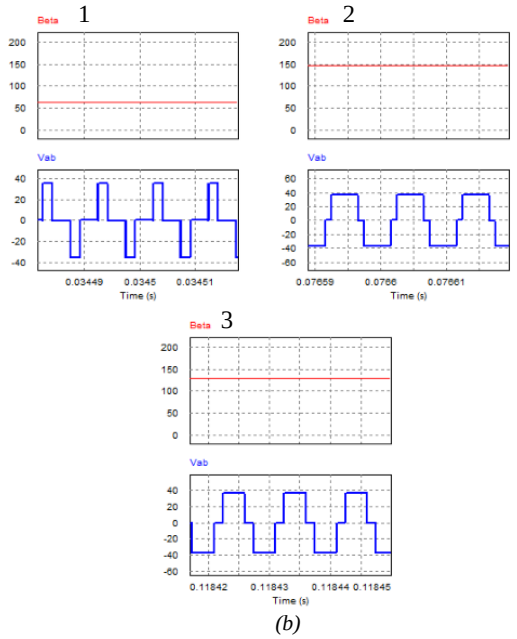

(b)

Fig. 6. Variation of PV power and phase shift angle for different irradiance values.

When Fig. 6 is analyzed, it is seen that the designed system follows the maximum power point with great accuracy. In addition, the variation of β with respect to the irradiance value and the variation of V_{ab} depending on the phase shift angle are presented in Fig. 6. When the solar irradiance value increases, the MPPT algorithm increases the effective value of the voltage applied to the resonance tank by increasing the phase shift angle. Thus, the load voltage and current increase. When the radiation value decreases, the maximum power value that can be obtained from the PV panel also decreases. Therefore, by decreasing the value of the β angle, the voltage applied to the resonant circuit and the load is reduced. In Fig. 7, under 300 W/m^2 solar irradiance value, resonance inductance current I_{Lr} magnetization current I_m values, drain-source voltages (Vds3, Vds4), gate voltages (Vgs_3, Vgs_4) and drain source currents of power switches S3 and S4 I(MOS3), I(MOS4) are presented.

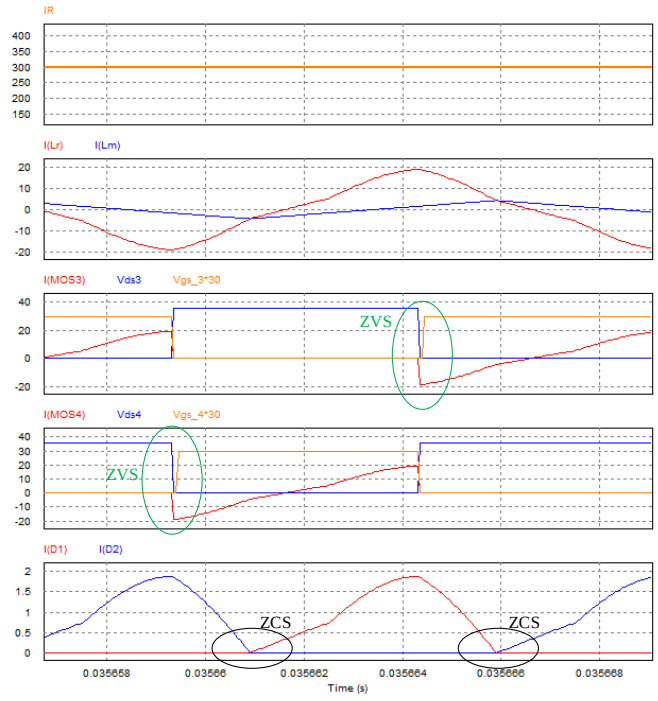

Fig. 7. ZVS and ZCS states for 300 W/m^2 irradiance value.

When Fig. 7 is analyzed, it is seen that the power switches S3 and S4 are conducting at ZVS. In the case where the current I_m is equal to the current I_{Lr}, no current flows through the primary of the transformer and no voltage is induced in the secondary part. During the time when both currents are equal to each other, the diode currents get a value of zero. Thus, the power diodes located on the secondary side are conducting in ZCS.

In Figure 8, ZVS and ZCS states are presented for solar irradiance values of 1000W/m^2 and 750W/m^2. When Fig. 7 and Fig. 8 are analyzed, it is seen that the power switches turn on in the ZVS condition and the power diodes turn on in the ZCS condition for all three irradiance values.

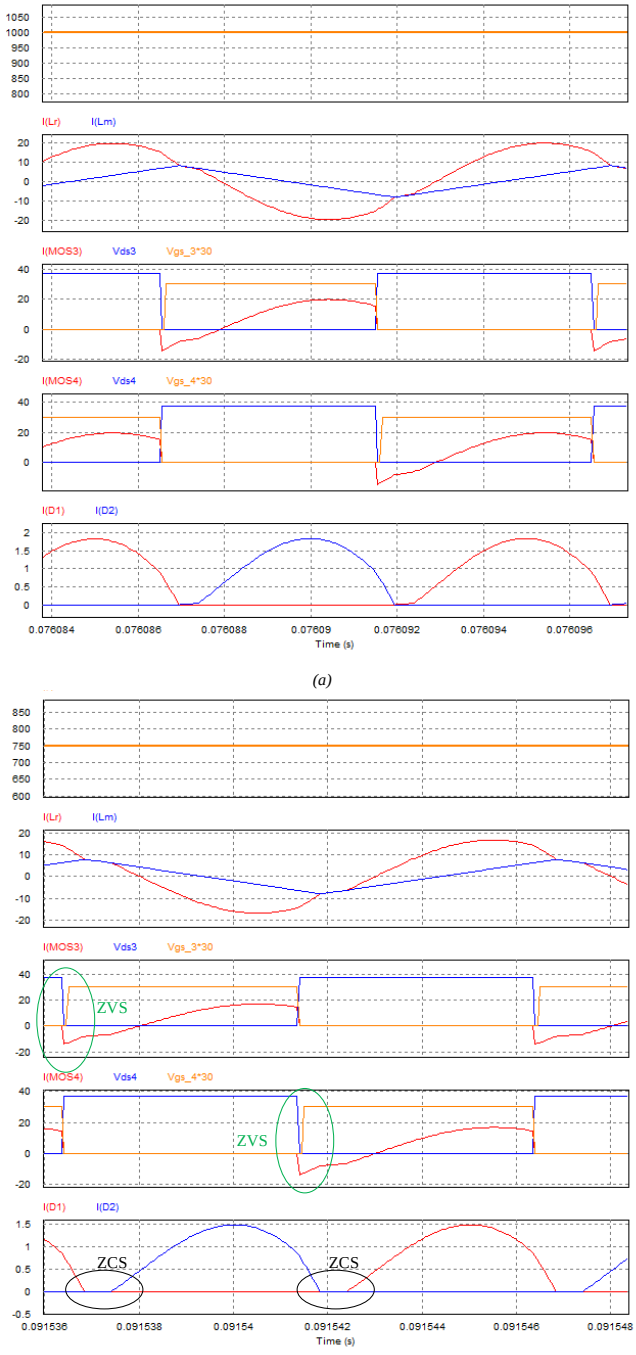

Fig. 8. ZVS and ZCS states for (a) 1000 W/m^2 (b) 750 W/m^2 irradiance values

VI. CONCLUSIONS

In this study, a 400Ω ohmic load is fed by using a single panel with a maximum power of 325.7W at 1000W/m^2 solar irradiance. In order to ensure that the designed PV system works under soft switching conditions and at MPP, a full-bridge LLC resonant converter is simulated. The switching frequency of the LLC resonant converter is chosen equal to the resonant frequency, so that the converter works in the inductive region. The P&O algorithm used as the MPPT algorithm is arranged according to the phase shift modulation technique. Phase-shift modulation method was chosen in the control of LLC resonant converter and operation at fixed switching frequency became possible. Operation at fixed

switching frequency simplifies magnetic design and reduces EMI problems. As can be seen from the simulation results, the designed system successfully follows the MPP under different solar irradiance conditions. In addition, under all radiation conditions, power switches S3 and S4 turn on under ZVS conditions and power diodes turn on under ZCS conditions. It is clearly seen from the simulation results that the designed system successfully achieves the expected targets under three solar irradiance conditions.

REFERENCES

[1] A. S. Ragab, N. H. Saad and A. A. El-Sattar, "LLC resonant DC-DC converter for grid-connected PV system," 2017 12th International Conference on Computer Engineering and Systems (ICCES), 2017, pp. 279-285.

[2] C. Buccella, C. Cecati, H. Latafat and K. Razi, "A grid-connected PV system with LLC resonant DC-DC converter," 2013 International Conference on Clean Electrical Power (ICCEP), 2013, pp. 777-782.

[3] C. Buccella, C. Cecati, H. Latafat and K. Razi, "Multi String Grid-Connected PV System with LLC Resonant DC/DC Converter" . Intell Ind Syst 1, 2015, pp. 37–49.

[4] A. Karafil, "Yarım köprü LLC rezonans dönüştürücünün analizi," 2nd International Eurasian Conference on Science, Engineering and Technology, 2020, pp. 135-142.

[5] Ozbay, H., "Rezonans Dönüştürücülü Fotovoltaik Batarya Şarj Sistemi", *Mühendislik Bilimleri ve Araştırmaları Dergisi*, *2*(1), 2020, pp. 11-20.

[6] Abdel-Rahim, O., Alamir, N., Orabi, M.et al.Fixed-frequency phase-shift modulated PV-MPPT for LLC resonant converters.J. PowerElectron.20,279–291, 2020.

[7] C. Chang, E. Chang and H. Cheng, "A High-Efficiency Solar Array Simulator Implemented by an LLC Resonant DC–DC Converter," in IEEE Transactions on Power Electronics, vol. 28, no. 6, pp. 3039-3046, June 2013.

[8] G. Bal, S. Oncu, N. Ozturk and K. Unal, "An Application of PDM Technique for MPPT in Solar Powered Wireless Power Transfer Systems," 2021 10th International Conference on Renewable Energy Research and Application (ICRERA), 2021, pp. 305-309.

[9] Y. Zhuang, F. Liu, X. Zhang, X. Diao, J. Jiang and J. Sun, "Direct Frequency Control Based MPPT Algorithm of LLC Resonant Converter for Photovoltaic System," 2019 IEEE Energy Conversion Congress and Exposition (ECCE), 2019, pp. 3402-3406.

[10] N. Alamir, M. A. Ismeil and M. Orabi, "New MPPT technique using phase-shift modulation for LLC resonant micro-inverter," 2017 Nineteenth International Middle East Power Systems Conference (MEPCON), 2017, pp. 1465-1470.

[11] S. M. Tayebi, H. Hu, S. Abdel-Rahman and I. Batarseh, "Dual-Input Single-Resonant Tank LLC Converter with Phase Shift Control for PV Applications," in IEEE Transactions on Industry Applications, vol. 55, no. 2, pp. 1729-1739, March-April 2019.

[12] X. Chen, S. M. Tayebi and I. Batarseh, "Efficiency Improvement of a Dual-input LLC Converter for PV Applications using Burst-mode Control Strategy," 2019 IEEE Energy Conversion Congress and Exposition (ECCE), 2019, pp. 6487-6494..

[13] Y. Wei, Q. Luo and A. Mantooth, "Overview of Modulation Strategies for LLC Resonant Converter," in IEEE Transactions on Power Electronics, vol. 35, no. 10, pp. 10423-10443, Oct. 2020.

[14] Q. Cao, Z. Li, B. Xue and H. Wang, "Fixed Frequency Phase Shift Modulated LLC Resonant Converter Adapted to Ultra Wide Output Voltage Range," 2019 IEEE Applied Power Electronics Conference and Exposition (APEC), 2019, pp. 817-822..

[15] N. Kollipara, M. K. Kazimierczuk, A. Reatti and F. Corti, "Phase Control and Power Optimization of LLC Converter," 2019 IEEE International Symposium on Circuits and Systems (ISCAS), 2019, pp. 1-5.

[16] K. Murata and F. Kurokawa, "Performance characteristic of interleaved LLC resonant converter with phase shift modulation," 2015 IEEE International Telecommunications Energy Conference (INTELEC), 2015, pp. 1-5.

[17] K. Murata and F. Kurokawa, "An Interleaved PFM LLC Resonant Converter With Phase-Shift Compensation," in IEEE Transactions on Power Electronics, vol. 31, no. 3, pp. 2264-2272, March 2016.

[18] B. McDonald and F. Wang, "LLC performance enhancements with frequency and phase shift modulation control," 2014 IEEE Applied Power Electronics Conference and Exposition - APEC 2014, 2014, pp. 2036-2040.

[19] Y. Wei, D. Woldegiorgis and A. Mantooth, "Control Strategies Overview for LLC Resonant Converter with Fixed Frequency Operation," 2020 IEEE 11th International Symposium on Power Electronics for Distributed Generation Systems (PEDG), 2020, pp. 63-68.

[20] M. Rashidi et al., "Design and Implementation of a LLC Resonant Solid-State Transformer," in IEEE Transactions on Industry Applications, vol. 56, no. 4, pp. 3855-3864, July-Aug. 2020.

[21] S. Oncu, S. Nacar, "Soft switching maximum power point tracker with resonant switch in PV system," international journal of hydrogen energy, 41(29), pp. 12477-12484, 2016.